Title
Differentiation of brain tumor-related edema based on 3D T1rho imaging

Authors
Villanueva-Meyer, JE
Barajas, RF
Mabray, MC
et al.

Publication Date
2017-06-01

DOI
10.1016/j.ejrad.2017.03.022

Peer reviewed

Published in final edited form as:

Eur J Radiol. 2017 June ; 91: 88–92. doi:10.1016/j.ejrad.2017.03.022.

Differentiation of brain tumor-related edema based on 3D T1rho imaging

J.E. Villanueva-Meyer[a], **R.F. Barajas Jr.**[b,g], **M.C. Mabray**[a], **W. Chen**[c], **A. Shankaranarayanan**[d], **P. Koon**[d], **I.J. Barani**[e], **T. Tihan**[f], and **S. Cha**[a,*]

[a]Department of Radiology and Biomedical Imaging, University of California San Francisco, San Francisco, CA, USA

[b]Department of Diagnostic Radiology, Oregon Health and Science University, Portland, OR, USA

[c]Department Imaging and Interventional Radiology, The Chinese University of Hong Kong, Prince of Wales Hospital, Shatin, NT, Hong Kong, China

[d]Global Applied Science Laboratory, GE Healthcare, Menlo Park, CA, USA

[e]Department of Radiation Oncology, University of California San Francisco, San Francisco, CA, USA

[f]Department of Pathology, University of California San Francisco, San Francisco, CA, USA

[g]Advanced Imaging Research Center, Oregon Health and Science University, Portland, OR, USA

Abstract

Background and purpose—Cerebral edema associated with brain tumors is an important source of morbidity. Its type depends largely on the capillary ultra-structures of the histopathologic subtype of underlying brain tumor. The purpose of our study was to differentiate vasogenic edema associated with brain metastases and infiltrative edema related to diffuse gliomas using quantitative 3D T1 rho (T1ρ) imaging.

Materials and methods—Preoperative MR examination including whole brain 3D T1ρ imaging was performed in 23 patients with newly diagnosed brain tumors (9 with metastasis, 8 with lower grade glioma, LGG, 6 with glioblastoma, GBM). Mean T1ρ values were measured in regions of peritumoral non-enhancing T2 signal hyperintensity, excluding both enhancing and necrotic or cystic component, and normal-appearing white matter.

Results—Mean T1ρ values were significantly elevated in the vasogenic edema surrounding intracranial metastases when compared to the infiltrative edema associated with either LGG or GBM ($p = 0.02$ and < 0.01, respectively). No significant difference was noted between T1ρ values of infiltrative edema between LGG and GBM ($p = 0.84$ and 0.96, respectively).

*Corresponding author at: 350 Parnassus Avenue, 370H, Department of Radiology and Biomedical Imaging, University of California San Francisco, San Francisco, CA 94143-0628, USA.

Conflict of interest

None.

Conclusion—Our study demonstrates the feasibility and potential diagnostic role of T1ρ in the quantitative differentiation between edema related to intracranial metastases and gliomas and as a potentially complementary tool to standard MR techniques in further characterizing pathophysiology of vasogenic and infiltrative edema.

Keywords

T1rho; Glioma; Metastasis; Peritumoral edema; Infiltrative edema; Vasogenic edema

1. Introduction

Cerebral edema is an important and common cause of morbidity in patients with brain tumors [1–3]. The type of cerebral edema depends on the histology of the brain tumor and is categorized as vasogenic, comprised of interstitial water, or infiltrative, containing both water and tumor cells [4,5]. Vasogenic edema is most commonly associated with intracranial metastases whereas infiltrative edema is seen with gliomas [4]. Differentiating the two types of edema on imaging can be challenging but is important for accurate preoperative diagnosis of tumor, guiding surgical resection, and monitoring treatment response [6].

Several MR imaging techniques, including diffusion, perfusion, and spectroscopy have been studied to distinguish vasogenic edema and infiltrative edema by providing quantitative measures of alterations in brain water signal, blood flow, and biochemical profiles, respectively [7,8]. T1ρ, or spin-lattice relaxation in the rotating frame, is a fast spin echo 3D sequence that employs a low frequency spin locking pulse with resultant increased sensitivity to slow lattice motions. T1ρ can be used to probe macromolecular interactions and has been shown to reflect normal aging as well as pathologic changes in tissue protein and pH content [9–11]. A small number of published reports have shown potential applications of T1ρ neuroimaging to evaluate tumor boundaries [12–16], neurodegenerative disease [17–19], demyelination [20,21], psychiatric disease [22], and acute cerebral ischemia [11,23,24].

The purpose of our study was to determine whether quantitative 3D T1ρ imaging could differentiate vasogenic edema and infiltrative edema. Because the paramount difference between vasogenic and infiltrative edema is the presence of infiltrating tumor cells in the latter, the low frequency interactions between macromolecules and bulk water were expected to be different between these two types of edema. We hypothesized that the higher water content and lack of tumor cells in vasogenic edema surrounding brain metastases would result in prolonged T1ρ values consistently throughout the region of vasogenic edema and hence distinguish it from infiltrative edema associated with infiltrating gliomas.

2. Materials and methods

2.1. Patient population

Twenty-three patients (11 men, 12 women; median age, 58 years, range 34–76 years) who presented for initial surgery of newly diagnosed brain tumor at our institution were recruited for preoperative MR examinations that included 3D T1ρ imaging. Evaluated patients were

divided into metastatic, LGG (WHO grade II and III), and GBM (WHO grade IV) tumor groups based on clinical history and/or pathology. All fourteen cases of glioma (LGG and GBM) as well as four of nine metastasis underwent surgical resection or biopsy with resultant histopathologically confirmed diagnosis. In the remaining five cases of metastasis, the diagnosis was presumed based on the clinical history of extracranial primary tumor and other whole-body imaging findings consistent with metastatic disease. This study was performed in accordance with the Health Insurance Portability and Accountability Act and received Institutional Review Board approval.

2.2. MR imaging protocol

All preoperative MR imaging including 3D T1ρ was performed on a 3.0 T clinical scanner (Discovery, GE Healthcare, Waukesha, WI). The MR imaging protocol included seven sequences: 3-plane localizer (TR/TE, 8.5/1.6 ms), sagittal T1-weighted spin-echo (TR/TE, 600/17 ms), axial 3D T2-weighted fast spin-echo (TR/TE, 3000/102 ms), axial FLAIR (TR/TE/TI, 10000/148/2200 ms), axial DWI echo-planar imaging (TR/TE, 10000/99 ms; section thickness/intersection gap, 5/0 mm; matrix size 256 × 256 × 24; FOV 24 cm; b-value, 1000 s/mm^2), 3D T1ρ, and contrast-enhanced 3D SPGR T1-weighted imaging (TR/TE, 34/8 ms; section thickness/intersection gap, 1.5/0 mm).

3D T1 ρ imaging was performed before the administration of intravenous gadolinium contrast using a magnetization prepared 3D pseudo steady-state fast spin echo acquisition pulse sequence. Imaging parameters included: 0.9 × 0.9 × 1.6 mm resolution, 280 × 196 mm FOV, 120 slices, 0.5 NEX, 2× ARC parallel imaging (GE Healthcare) along the phase encoding direction, echo train length of 12, spin lock frequency 500 Hz, and time of spin lock (TSL) 2, 10, 40, 60, 80, and 100 ms. The total scan time for T1ρ data acquisition was 3.5 min MR image processing.

2.3. MR imaging processing and T1ρ measurements

The FLAIR, T1ρ, and contrast-enhanced 3D SPGR images were transferred to a commercially available post-processing workstation (Advantage Workstation, GE Healthcare). Image processing was performed in a blinded manner using commercially available software (FuncTool 9.4.05a, GE Healthcare).

Using FuncTool (GE Healthcare) T2 mapping software, the acquired 3D T1ρ image data sets were fitted to a mono-exponential model using least square fit to obtain T1ρ or T2 value within the ROI. We chose a small (50 mm^2) ROI within a normal appearing white matter contralateral to the tumor hemisphere for fitting. A predefined threshold, as part of the software workflow, was designed to limit the bias in T2 calculation due to the background noise contribution with the late echoes. The lower the value of confidence, the tighter the condition on the mono-exponential fit. FuncTool T2 mapping is based on least square fitting to a mono-exponential decay model with a truncation method as follows: (1) Selects the first 3 echoes and takes the logarithm; if true mono-exponential decay, then we get a linear fit of the 3 echoes; (2) Calculates linear regression coefficient R; (3) Adds the next echo of the curve, linearizes and determines R'; (4) If R' does not differ by more than a predefined threshold, then it continues the iteration with next echoes until the end of the echoes or until

the condition is no longer met; (5) If R'-R exceeds the predefined threshold, then the calculation is stopped. If this happens at the very first iteration, then the pixel is blacked out.

Once the T1ρ maps were calculated on a voxel-by-voxel basis from the T1ρ imaging sets, they were aligned with FLAIR and contrast-enhanced 3D SPGR images in the same axial location and resolution. For each trans-axial plane of T1ρ, co-registered ROIs were manually defined around non-contrast-enhancing T2/FLAIR abnormality (NCE) and contralateral normal appearing white matter (NAWM) allowing T1ρ measurement.

Within the ROIs, none of the patients demonstrated evidence of blood products or other confounding factors that could have effects on the quantitative metrics. ROIs were manually corrected on the T1ρ maps to avoid regions of contrast enhancement and cystic/necrotic change. Volumes of NCE tumor were calculated from ROI analysis. Generation of ROIs allowed for the collection of mean values for each ROI per axial slice. The individual means were then weighted by ROI area to calculate the average of the mean T1ρ values for the NCE ROIs from the entirety of peritumoral edema. All ROIs were subsequently approved by an attending neuroradiologist certified by the American Board of Radiology with a Certificate of Added Qualification in neuroradiology.

2.4. Statistical analysis

All T1ρ values are measured and reported in milliseconds. Descriptive statistics were performed to calculate the mean and 95% confidence interval of T1ρ and ADC values in the different study groups. One-way analysis of variance was performed to compare NCE volumes, mean NCE T1ρ and ADC values, and mean NAWM T1ρ and ADC values between tumor groups. Post hoc comparisons were performed using the Bonferroni-Holm method. A p-value of less than 0.05 was considered statistically significant.

3. Results

3.1. Patient characteristics

Table 1 summarizes the characteristics of the evaluated tumor patients. All metastasis, five of eight LGG, and all GBM patients examined in this study demonstrated contrast enhancement. All patients enrolled in this study had evidence of NCE peritumoral edema. Mean volume of NCE peritumoral edema was 44.5 cm^3 in metastases, 49.3 cm^3 in LGGs, and 29.2 cm^3 in GBMs; no significant difference was observed between the groups (p = 0.36). Representative cases of metastasis, LGG, and GBM are shown in Fig. 1.

3.2. T1ρ measurements

Differences in mean T1ρ values between metastases, LGGs, and GBMs are reported in Table 2 and depicted in Fig. 2. Mean T1ρ values were significantly elevated in NCE of metastases compared to those in LGGs and GBMs by one-way ANOVA (p = 0.018). Bonferroni-Holm post-hoc tests revealed differences between the mean T1ρ values in NCE of metastases compared to LGGs (p = 0.034) and GBMs (p = 0.040). No significant difference was observed between mean T1ρ values in NCE of LGGs compared to GBMs (p = 0.964). In Fig. 3. examples of histograms from selected axial ROIs in metastatic tumor and glioma are

shown. Overall, histograms of T1ρ values were higher and narrower in the metastasis group compared to the gliomas. Mean NAWM T1ρ values were 78.9 in metastasis, 78.6 in LGG, and 78.2 in GBM. No significant difference was found between T1ρ values in NAWM across the tumor groups ($p = 0.914$). Compared to regions of peritumoral edema, NAWM T1ρ was significantly different in all tumor groups ($p < 0.001$).

4. Discussion

In this study we used whole brain 3D T1ρ imaging to quantitatively assess and differentiate two types of cerebral edema caused by brain tumors—vasogenic edema associated with brain metastases and infiltrative edema associated with infiltrating gliomas. We found significantly higher T1ρ values in the vasogenic edema of brain metastases compared to the infiltrative edema of gliomas. Our study suggests that T1ρ imaging may be capable of capturing and quantifying the pathophysiologic difference between vasogenic and infiltrative edema.

To the best of our knowledge, whole brain T1ρ imaging has not been previously used to characterize the pathological processes of untreated brain tumors and associated cerebral edema in humans. T1ρ has been studied to a limited extent in several neuroimaging applications including the evaluation of ischemia [11,23,24], neurodegenerative disorders [17,18], demyelinating disease [20,21], animal models of brain tumor [12–14,25], and response to gene therapy [15,16]. Although the exact mechanisms governing T1ρ relaxation are not fully understood, several factors proposed to influence T1ρ include scalar coupling, dipole–dipole interactions, and chemical exchange processes [26]. Our findings of difference in mean T1ρ values between the two types of tumor-related edema can be interpreted in the context of the aforementioned studies and current understanding of tumor pathophysiology. We suggest that in peritumoral edema, the dominant factor influencing T1ρ is the macromolecular content of the extracellular environment. In purely vasogenic edema, where there is an increased ratio of water to protein, we observed T1ρ prolongation. Conversely, we noted relative T1ρ shortening in infiltrative peritumoral edema due to increased macromolecular content associated with infiltrative tumor cells. This is consistent with *in vitro* [27] and *in vivo* [28] studies demonstrating decreased T1ρ values with increasing concentration of macromolecular content in solution or in tissue, respectively.

As evidenced by the broader histogram distribution and wider interquartile range on the boxplots, we observed a broader range of variability in T1ρ values within the peritumoral edema of LGG and GBM compared to that of metastatic tumors. This may reflect the heterogeneous nature of infiltrative edema associated with glial tumors versus the largely isolated increased bulk water of metastasis. These findings were seen across both glioma groups and we found no significant difference in T1ρ values of edema between LGG and GBM. While some of the elevated values in infiltrative edema can be explained by lower cellularity and greater water content, other physiologic processes may underlie the observed T1ρ values. For example, studies of cerebral ischemia have suggested that T1ρ prolongation in ischemic regions relates to higher acidity caused by ischemic or infarcted tissue leading to altered proton exchange and macromolecular integrity [24,29]. Acidic extracellular pH from tumor catabolism has been observed in brain tumors and as such we postulate that proton

exchange may play a central role in the observations [30,31]. A review of the literature does not reveal any studies evaluating tumor pH differences between metastases and gliomas. Our findings may reflect differences in metabolism related to tumor grade in gliomas and primary tumor characteristics in metastases.

Based on our preliminary study, 3D T1ρ imaging may be a useful complimentary metric for evaluating different types of brain tumors. Using this technique, high-resolution T1ρ maps can be fused with standard morphologic MR images to provide quantitative values for more precise regional assessment and longitudinal comparison. T1ρ is a high spatial resolution technique that could potentially be used to direct real-time image-guided biopsy. This intraoperative application has a potentially high clinical impact for the management of patients with glioma. If validated by prospective studies with pathologic correlation, T1ρ MR imaging could be used to delineate the infiltrating tumor margin with resultant alterations to surgical approach or radiation field planning.

Our study had several limitations including its small sample size and retrospective design and should be considered a preliminary study. Additionally, while most of the tumor diagnoses were confirmed pathologically, there was no direct imaging and pathology correlation based on T1ρ values and image-guided tissue biopsy results to better define the underlying biology of T1ρ alteration. To prospectively validate and identify tissue correlates of T1ρ, future studies will include tissue biopsy using image-guided approach to directly correlate tissue characteristics with T1ρ and other quantitative MR imaging parameters. A larger sample size and prospective pathologic correlation would allow for more robust comparison between tumor groups, help establish meaningful cutoff values for T1ρ measurements, and potentially lead to changes in patient management.

5. Conclusion

Our study demonstrates the clinical feasibility and potential role of T1ρ imaging in the quantitative assessment and differentiation of vasogenic edema caused by brain metastases and infiltrative edema associated with infiltrating gliomas. Image-guided tissue biopsy directed by T1ρ imaging may be the next step towards validation and identification of tissue and biologic correlates of altered T1ρ values in different types of tumor-related edema and cellular heterogeneity of various brain tumors.

Acknowledgments

Funding

This work was supported by the National Institutes of Health T32 Grant (5 T32 EB001631-12)

Abbreviations

GBM	glioblastoma
LGG	lower grade glioma
NAWM	normal appearing white matter

NCE	non-enhancing T2 signal hyperintensity
WHO	World Health Organization

References

1. Surawicz TS, McCarthy BJ, Kupelian V, et al. Descriptive epidemiology of primary brain and CNS tumors: results from the central brain tumor registry of the United States, 1990–1994. Neuro Oncol. 1999; 1(1):14–25. [PubMed: 11554386]
2. Porter KR, McCarthy BJ, Freels S, Kim Y, Davis FG. Prevalence estimates for primary brain tumors in the United States by age, gender, behavior, and histology. Neuro Oncol. 2010; 12(6):520–527. [PubMed: 20511189]
3. Davis FG, Dolecek TA, McCarthy BJ, Villano JL. Toward determining the lifetime occurrence of metastatic brain tumors estimated from 2007 United States cancer incidence data. Neuro Oncol. 2012; 14(9):1171–1177. [PubMed: 22898372]
4. Walter, Stummer. Mechanisms of tumor-related brain edema. Neurosurg. Focus. 2007; 22.5:1–7.
5. Nag S, Manias JL, Stewart DJ. Pathology and new players in the pathogenesis of brain edema. Acta Neuropathol. 2009; 118(2):197–217. [PubMed: 19404652]
6. Cha S, Lupo JM, Chen MH, et al. Differentiation of glioblastoma multiforme and single brain metastasis by peak height and percentage of signal intensity recovery derived from dynamic susceptibility-weighted contrast-enhanced perfusion MR imaging. Am. J. Neuroradiol. 2007; 28(6): 1078–1084. [PubMed: 17569962]
7. Oh J, Cha S, Aiken AH, et al. Quantitative apparent diffusion coefficients and T2 relaxation times in characterizing contrast enhancing brain tumors and regions of peritumoral edema. J. Magn. Reson. Imaging. 2005; 21(6):701–708. [PubMed: 15906339]
8. Moseley ME, Butts K, Yenari MA, Marks M, Crespigny AD. Clinical aspects of DWI. NMR Biomed. 1995; 8(7):387–396. [PubMed: 8739275]
9. Redfield AG. Nuclear spin thermodynamics in the rotating frame. Science. 1969; 164(3883):1015–1023. [PubMed: 17796604]
10. Watts R, Andrews T, Hipko S, Gonyea JV, Filippi CG. In vivo whole-brain T1-rho mapping across adulthood: normative values and age dependence. J. Magn. Reson. Imaging. 2013; 40(2):376–382. [PubMed: 24227659]
11. Magnotta VA, Heo HY, Dlouhy BJ, et al. Detecting activity-evoked pH changes in human brain. Proc. Natl. Acad. Sci. 2012; 109(21):8270–8273. [PubMed: 22566645]
12. Aronen HJ, Abo Ramadan U, Peltonen TK, et al. 3D spin-lock imaging of human gliomas. Magn. Reson. Imaging. 1999; 17(7):1001–1010. [PubMed: 10463651]
13. Markkola AT, Aronen HJ, Paavonen T, et al. T1ρ dispersion imaging of head and neck tumors: a comparison to spin lock and magnetization transfer techniques. J. Magn. Reson. Imaging. 1997; 7(5):873–879. [PubMed: 9307914]
14. Poptani H, Duvvuri U, Miller CG, et al. T1ρ imaging of murine brain tumors at 4 T. Acad. Radiol. 2001; 8(1):42–47. [PubMed: 11201456]
15. Hakumäki JM, Gröhn OH, Tyynelä K, Valonen P, Ylä-Herttuala S, Kauppinen RA. Early gene therapy–induced apoptotic response in BT4C gliomas by magnetic resonance relaxation contrast T1 in the rotating frame. Cancer Gene Ther. 2002; 9(4):338–345. [PubMed: 11960284]
16. Kettunen MI, Kettunen MI, Sierra A, et al. Low spin-lock field T1 relaxation in the rotating frame as a sensitive MR imaging marker for gene therapy treatment response in rat glioma 1. Radiology. 2007; 243(3):796–803. [PubMed: 17517934]
17. Borthakur A, Sochor M, Davatzikos C, Trojanowski JQ, Clark CM. T1ρ MRI of Alzheimer's disease. Neuroimage. 2008; 41(4):1199–1205. [PubMed: 18479942]
18. Haris M, Singh A, Cai K, et al. T1rho (T1ρ) MR imaging in Alzheimer' disease and Parkinson's disease with and without dementia. J. Neurol. 2010; 258(3):380–385. [PubMed: 20924593]
19. Haris M, Yadav SK, Rizwan A, et al. T1rho MRI and CSF biomarkers in diagnosis of Alzheimer's disease. YNICL. 2015; 7(C):598–604.

20. Mangia S, Carpenter AF, Tyan AE, Eberly LE, Garwood M, Michaeli S. Magnetization transfer and adiabatic T1ρ MRI reveal abnormalities in normal-appearing white matter of subjects with multiple sclerosis. Mult. Scler. J. 2014; 20(8):1066–1073.
21. Gonyea JV, Watts R, Applebee A, et al. In vivo quantitative whole-brain T 1rho MRI of multiple sclerosis. J. Magn. Reson. Imaging. 2015; 42(6):1623–1630. [PubMed: 26032694]
22. Johnson CP, Follmer RL, Oguz I, et al. Brain abnormalities in bipolar disorder detected by quantitative T1ρ mapping. Mol. Psychiatry. 2015; 20(2):201–206. [PubMed: 25560762]
23. Jokivarsi KT, Hiltunen Y, Grohn H, Tuunanen P, Grohn OHJ, Kauppinen RA. Estimation of the onset time of cerebral ischemia using T1ρ and T2 MRI in rats. Stroke. 2010; 41(10):2335–2340. [PubMed: 20814006]
24. Gröhn OH, Kettunen MI, Mäkelä HI, et al. Early detection of irreversible cerebral ischemia in the rat using dispersion of the magnetic resonance imaging relaxation time, T1rho. J. Cereb. Blood Flow Metab. 2000; 20(10):1457–1466. [PubMed: 11043908]
25. Sepponen RE, Pohjonen JA, Sipponen JT, Tanttu JI. A method for Tlp imaging. J. Comput. Assist. Tomogr. 1985; 9(6):1007–1011. [PubMed: 4056129]
26. Borthakur A, Mellon E, Niyogi S, Witschey W, Kneeland JB, Reddy R. Sodium and T1ρ MRI for molecular and diagnostic imaging of articular cartilage. NMR Biomed. 2006; 19(7):781–821. [PubMed: 17075961]
27. Virta A, Komu M, Kormano M. T1rho of protein solutions at very low fields: dependence on molecular weight, concentration, and structure. Magn. Reson. Med. 1997; 37(1):53–57. [PubMed: 8978632]
28. Li X, Benjamin Ma C, Link TM, et al. In vivo T1ρ and T2 mapping of articular cartilage in osteoarthritis of the knee using 3T MRI. Osteoarthritis Cartilage. 2007; 15(7):789–797. [PubMed: 17307365]
29. Gröhn OH, Lukkarinen JA, Silvennoinen MJ, Pitkänen A, van Zijl P, Kauppinen RA. Quantitative magnetic resonance imaging assessment of cerebral ischemia in rat using on-resonance T1 in the rotating frame. Magn. Reson. Med. 1999; 42(2):268–276. [PubMed: 10440951]
30. Zhang X, Lin Y, Gillies RJ. Tumor pH and its measurement. J. Nucl. Med. 2010; 51(8):1167–1170. [PubMed: 20660380]
31. Martinez GV, Zhang X, García-Martín ML, et al. Imaging the extracellular pH of tumors by MRI after injection of a single cocktail of T1and T2 contrast agents. NMR Biomed. 2011; 24(10):1380–1391. [PubMed: 21604311]

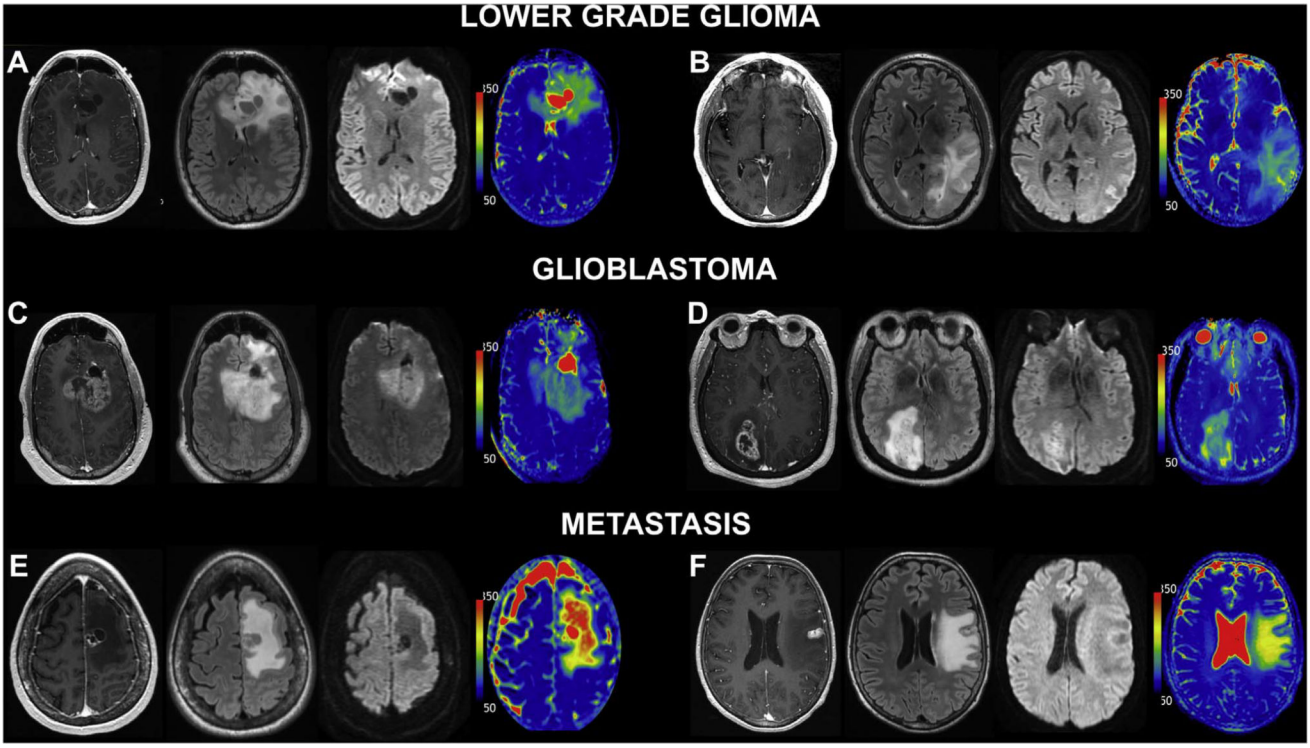

Fig. 1.

T1ρ differentiates glial neoplasm from intraparenchymal metastatic disease. Six representative patients from the three studied tumor groups; imaging from right to left: post-contrast 3D T1 SPGR, FLAIR, DWI (T2 trace image), and T1ρ color map. LGG: (A) 41-year-old man with anaplastic astrocytoma (WHO grade III) and (B) 57-year-old man with oligoastrocytoma (WHO grade II). GBM: (C) 52-year-old man and (D) 76-year-old woman with GBM (WHO grade IV). Metastatic disease: (E) 64-year-old woman with small cell lung carcinoma metastasis and (F) 67-year-old woman with metastatic breast cancer. Similar morphologic appearance is demonstrated on post-contrast 3D T1 SPGR, FLAIR, and DWI images. Markedly increased T1ρ values are observed within the NCE peritumoral edema portion of the intracranial metastasis. Conversely, the gliomas demonstrate decreased T1ρ within the NCE pertiumoral edema when compared to metastatic disease. This observation across the imaging cohort was found to be statistically significant. Note elevated T1ρ values within the increased bulk water of the cystic/necrotic components in (A), (C), and (E).

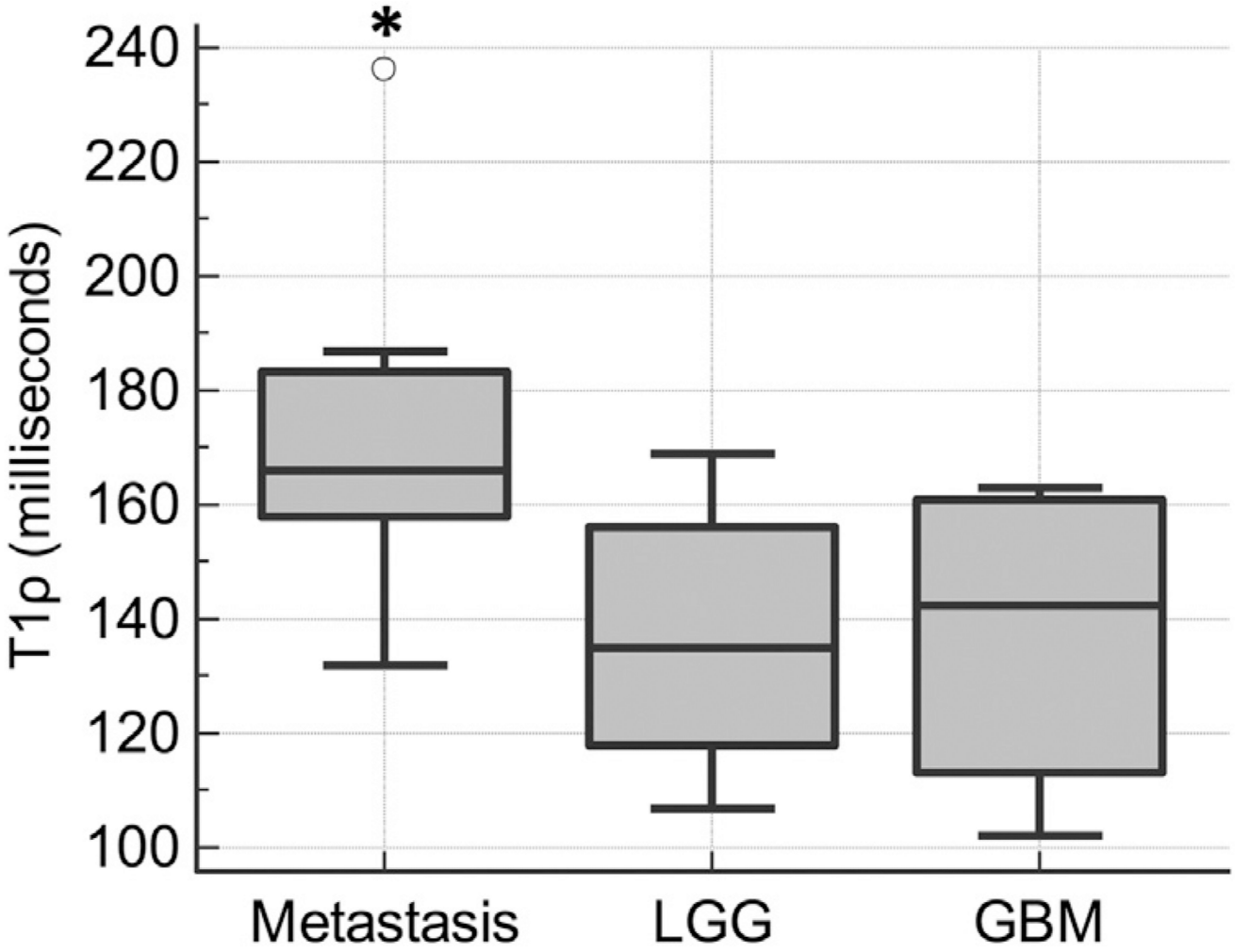

Fig. 2.

Boxplots of mean T1ρ in NCE between tumor groups. Quantitative T1ρ values were significantly higher in metastasis compared to LGG and GBM (*). There was no significant difference in T1ρ values between LGG and GBM.

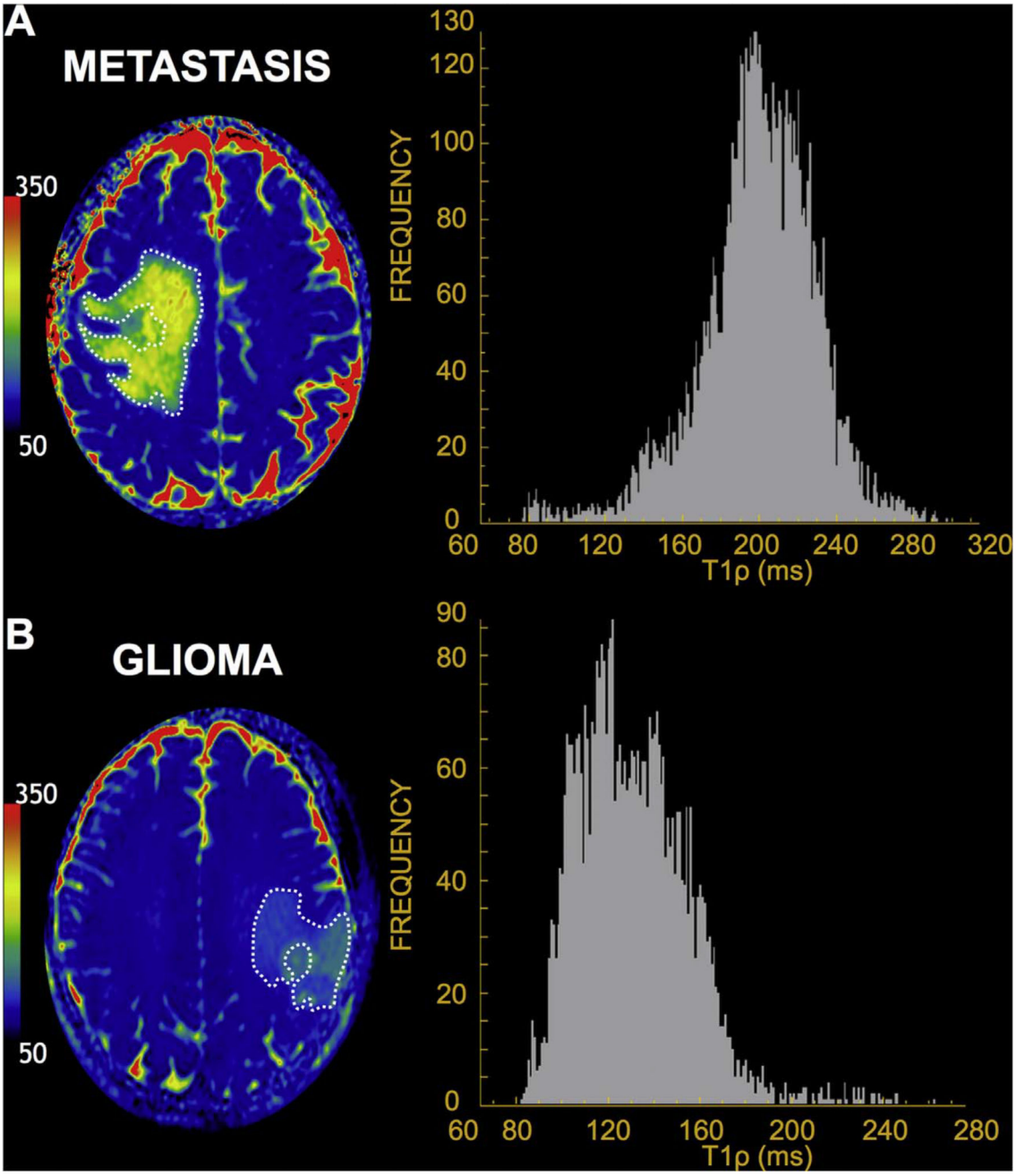

Fig. 3.

Representative T1ρ color maps and axial NCE ROI histograms. A rightward deviation and a narrower histogram of T1ρ value frequencies in the NCE of (A) 59-year-old man with lung adenocarcinoma metastasis is seen compared to that of a (B) 34-year-old man with anaplastic astrocytoma.

Table 1

Clinical and pathologic patient characteristics.

Patient	Age/Sex	Pathology	Tumor Group
1	64/F	Colon	Metastasis
2	59/M	Lung (Small Cell)	Metastasis
3	52/M	Lung (Adenocarcinoma)	Metastasis
4	70/M	Prostate	Metastasis
5	58/F	Presumed Breast	Metastasis
6	71/M	Presumed Melanoma	Metastasis
7	37/F	Presumed Breast	Metastasis
8	67/F	Presumed Breast	Metastasis
9	59/F	Presumed Endometrial	Metastasis
10	41/M	OA (WHO II)	LGG
11	57/M	OA (WHO II)	LGG
12	47/F	AO (WHO III)	LGG
13	62/F	AO (WHO III)	LGG
14	54/F	AA (WHO III)	LGG
15	34/M	AA (WHO III)	LGG
16	34/M	OA (WHO II)	LGG
17	73/M	DA (WHO II)	LGG
18	52/M	GBM (WHO IV)	GBM
19	59/F	GBM (WHO IV)	GBM
20	56/M	GBM (WHO IV)	GBM
21	70/F	GBM (WHO IV)	GBM
22	50/F	GBM (WHO IV)	GBM
23	76/F	GBM (WHO IV)	GBM

Note: OA, oligoastrocytoma; AO, anaplastic oligodendroglioma; AA, anaplastic astrocytoma; DA, diffuse astrocytoma; LGG, lower grade glioma; GBM, glioblastoma.

Table 2

Comparison of MR imaging findings.

Tumor Group	Mean $T1\rho_{NCE}$ (95% CI)
Metastasis (N = 9)	171.7 (152.7–190.7)
LGG (N = 8)	136.8 (121.5–152.1)
GBM (N = 6)	137.3 (117.3–157.3)
p-value *	0.018

NCE, non-contrast-enhancing T2/FLAIR abnormality; T1ρ values are reported in ms.

* By one-way ANOVA.